Ultra-high sensitivity optical stress sensor based on double-layered photonic crystal microcavity

Tsan-Wen Lu* and Po-Tsung Lee

Department of Photonics and Institute of Electro-Optical Engineering, National Chiao Tung University
Rm. 415, CPT Building, 1001 Ta Hsueh Road, 300 Hsinchu, Taiwan, R.O.C.
ricky.eo94g@nctu.edu.tw

Abstract: In this report, we present the design principles to achieve a highly sensitive optical stress sensor. The structure we use is a double-layered (DL) photonic molecule with optical bonding and anti-bonding states based on whispering-gallery mode in photonic crystal microcavity. By applying finite-difference time-domain and finite-element methods, we simulate the change of optical properties (including wavelength and quality (Q) factor) of bonding mode caused by the DL structural variation due to the applied stress in two DL geometries. In the end, we summarize an optical stress sensor design with high Q factor, large structural response due to the applied stress, and large optical spectrum change due to the DL structural variation. The minimum detectable stress variation is estimated to be as small as 0.95 nN.

OCIS codes: (230.5298) Photonic crystals; (140.3945) Microcavities

References and links

1. E. Yablonovitch, "Inhibited Spontaneous Emission in Solid-State Physics and Electronics," Phy. Rev. Lett. **58**, 2059-2062 (1987).
2. O. Painter, P. K. Lee, A. Scherer, A. Yariv, J. D. O'Brien, P. D. Dapkus, and I. Kim, "Two-Dimensional Photonic Band-Gap Defect Mode Laser," Science **284**, 1819-1821 (1999).
3. S. Noda, M. Fujita, and T. Asano, "Spontaneous-emission control by photonic crystals and nanocavities," Nature Photon. **1**, 449-458 (2007).
4. K. Nozaki, S. Kita, and T. Baba, "Room temperature continuous wave operation and controlled spontaneous emission in ultrasmall photonic crystal nanolaser," Opt. Express **15**, 7506-7514 (2007).
5. S. Kita, K. Nozaki, and T. Baba, "Refractiveindex sensing utilizing a cw photonic crystal nanolaser and its array configuration," Opt. Express **16**, 8174-8180 (2008).
6. S. H. Kwon, T. Sunner, M. Kamp, and A. Forchel, "Optimization of photonic crystal cavity for chemical sensing," Opt. Express **16**, 11709-11717 (2008).
7. M. Adams, G. A. DeRose, M. Loncar, and A. Scherer, "Lithographically fabricated optical cavities for refractive index sensing," J. Vac. Sci. Technol. B **23**, 3168-3173 (2005).
8. T. Sunner, T. Stichel, S. H. Kwon, T. W. Schlereth, S. Hofling, M. Kamp, and A. Forchel, "Photonic crystal cavity based gas sensor," Appl. Phys. Lett. **92**, 261112 (2008).
9. M. R. Lee and P. M. Fauchet, "Nanoscale microcavity sensor for single particle detection," Opt. Lett. **32**, 3284-3286 (2007).
10. F. Vollmer anf S. Arnold, "Whispering-gallery-mode biosensing: label-free detection down to single molecules," Nature Methods **5**, 591-596 (2008).
11. W. Suh, M. F. Yanik, O. Solgaard, and S. Fan, "Displacement-sensitive photonic crystal structures based on guided resonance in photonic crystal slabs," Appl. Phys. Lett. **82**, 1999-2001 (2003).
12. C. K. Lee, R. Radhakrishnan, C. C. Chen, J. Li, J. Thillaigovindan, and N. Balasubramanian, "Design and Modeling of a Nanomechanical Sensor Using Silicon Photonic Crystals," IEEE J. Lightwave Technol. **26**, 839-846 (2008).
13. C. K. Lee, J. Thillaigovindan, C. C. Chen, X. T. Chen, Y. T. Chao, S. Tao, W. Xiang, H. Feng, and G. Q. Lo, "Si nanophotonics based cantilever sensor," Appl. Phys. Lett. **93**, 113113 (2008).
14. O. Levy, B. Z. Steinberg, M. Nathan, and A. Boag, "Ultrasensitive displacement sensing using photonic crystal waveguides," Appl. Phys. Lett. **86**, 104102 (2005).
15. Z. Xu, L. Cao, C. Gu, Q. He, and G. Jin, "Micro displacement sensor based on line-defect resonant cavity in photonic crystal," Opt. Express **14**, 298-305 (2006).

#104267 - $15.00 USD Received 18 Nov 2008; revised 26 Dec 2008; accepted 8 Jan 2009; published 26 Jan 2009

16. P. T. Lee, T. W. Lu, C. M. Yu, and C. C. Tseng, "Photonic crystal circular-shaped microcavity and its uniform cavity-waveguide coupling property due to presence of whispering gallery mode," Opt. Express **15**, 9450-9457 (2007).
17. M. D. Barnes, S. M. Mahurin, A. Mehta, B. G. Sumpter, and D. W. Noid, "Three-dimensional photonic "molecules" from sequentially attached polymer-blend microparticles," Phys. Rev. Lett. **88**, 015508 (2002).
18. M. Bayer, T. Gutbrod, J. P. Reithmaier, and A. Forchel, "Optical Modes in Photonic Molecules," Phys. Rev. Lett. **81**, 2582-2585 (1998).
19. A. Nakagawa, S. Ishii, and T. Baba, "Photonic molecule laser composed of GaInAsP microdisks," Appl. Phys. Lett. **86**, 041112 (2005).
20. Y. Kanamori, T. Kitani, and K. Hane, "Control of guided resonance in a photonic crystal slab using microelectromechanical actuators," Appl. Phys. Lett. **90**, 031911 (2007).
21. G. H. Kim, Y. H. Lee, A. Shinya, and M. Notomi, "Coupling of small, low-loss hexapole mode with photonic crystal slab waveguide mode," Opt. Express **12**, 6624-6631 (2004).
22. H. Tnaiyama, M. Notomi, E. Kuramochi, T. Yamamoto, Y. Yoshikawa, Y. Torii, and T. Kuga, "Strong radiation force in two-dimensional photonic crystal slab cavities," Phys. Rev. B **78**, 165129 (2008).
23. E. Kuramochi, H. Taniyama, T. Tanabe, A. Shinya, and M. Notomi, "Ultrahigh-*Q* two-dimensional photonic crystal slab nanocavities in very thin barriers," Appl. Phys. Lett. **93**, 111112 (2008).
24. Y. Tanaka, T. Asano, and S. Noda, "Design of photonic crystal nanocavity with Q-factor of similar to 10^9," IEEE J. Lightwave Technol. **26**, 1532-1539 (2008).

1. Introduction

Over the past hundred years, people have shown high interests and researched in various light wave properties including reflections, refractions, diffractions, interferences, and so on. By building various optical sensing systems, people can measure different material properties such as index, thickness, deformation, and bending through the variations of these optical properties. In recent decades, attributing to the mature of micro-fabrication technologies, the optical micro-electromechanical systems (MEMS) are widely developed for various versatile optical sensors in micro-chip scale with fine or even higher sensitivity than that in conventional ones. By the associations of optical waveguides, microcavities, and other micro-structures, optical sensors in micro-chip scale have been widely applied in various fields, especially in biological, mechanical, and chemical developments. However, when people want to further minimize the system to be operated in wavelength scale, the huge obstacle, serious optical losses caused by total-internal-reflection (TIR) in wavelength scale, blocks up the way cruelly.

In 1987, the concept of photonic crystal (PhC) proposed by E. Yablonovitch [1], which represents the material with periodic index arrangement, opens up another opportunity and possibility for people to control light wave in wavelength scale by its photonic band-gap (PBG) effect. In recent years, a great deal of reports have indicated that PhCs with PBG can efficiently control the light wave behaviors in wavelength scale, for example, spontaneous emissions in microcavities, light propagations in waveguides, negative refractions, and so on. Since O. Painter *et al.* firstly demonstrated the PhC microcavity in 1999 [2], it has been regarded as a key component in constructing versatile photonic integrated chips. Due to the high quality (Q) factor [3] and small mode volume [4] in PhC microcavity, it is potential in achieving advantages of highly sensitive, portable, condensed, and so on, for serving as optical sensors. Very recently, highly sensitive optical index and particle sensors have been investigated and reported by several groups [5-9] based on PhC micro- and nano-cavities with ultra-small mode volume and high Q factors, which are potential in chemical sensing and biological labeling [10]. On the other hand, optical stress sensor is another important component in mechanical and semiconductor applications, especially in MEMS. Although some interesting optical stress sensor designs based on PhCs or PhC waveguides have been reported [11-15], the designs based on high Q micro- or nano-cavities are still hard to find in literatures and the sensitivity of present designs can be further improved. In this report, first we will briefly illustrate the design principles of a highly sensitive optical stress sensor. According to the requirements, we will introduce a structural design based on photonic molecule composed of doubled-layered (DL) PhC microcavity with high Q whispering-gallery (WG) mode. The basic modal properties and optical spectrum response for structural

#104267 - $15.00 USD Received 18 Nov 2008; revised 26 Dec 2008; accepted 8 Jan 2009; published 26 Jan 2009

variations of DL PhC microcavity will be investigated by three-dimensional (3D) finite-difference time-domain (FDTD) simulations. Then we will propose two DL geometric designs. The relationship between applied stress and corresponding structural variation will be calculated and analyzed by finite-element method (FEM). Finally, combining the results from FEM and FDTD simulations, we can summarize an optical stress sensor design with ultra-high sensitivity.

2. Design principles

Generally, in optical stress sensors, according to the measured optical property change due to the structural variation, one can estimate the applied stress that leads to the corresponding structural variation. Among present reports of PhC optical stress sensors, we can roughly classify them into two categories by the detected optical property variations, optical spectrum and intensity. In the former one, researchers can measure the optical transmission spectrum shift caused by the displacement between PhC membranes [11] or by the elongated cavity length in microcavity-waveguide system on cantilever and suspended PhC membranes [12, 13] to estimate the applied stress on these structures. In the latter one, researchers can measure the transmitted optical intensity degradation due to the waveguides misalignment [14, 15] caused by the applied stress. However, in real case, there will be larger inaccuracy in measuring optical intensity variation than optical spectrum shift. Thus, estimating applied stress by optical spectrum shift would be a better and promising approach. Generally, at first, researchers can find the relationship between the applied stress and the corresponding structural variation of their designed structure, for example, membrane displacement in ref. [11] and elongation of microcavity in ref. [12]. And then the relationship between the structural variation and the corresponding optical spectrum shift will be addressed. According to these two relationships, one can estimate the applied stress by the measured optical spectrum shift and decide how small the detectable stress variation per wavelength unit (F_{det}, defined as detectable stress variation in newton unit per optical wavelength shift in nanometer, that is, N / nm) is. We can define a simple equation to illustrate this relationship:

$$F_{\det} = \frac{\Delta F}{\Delta \lambda} = \frac{\Delta F}{\Delta d} \times \frac{\Delta d}{\Delta \lambda} \tag{1}$$

where $\Delta F / \Delta d$ represents the applied stress needed to cause specific structural variation and $\Delta d / \Delta \lambda$ represents the structural variation needed to cause specific optical spectrum shift, respectively. From equation (1), we find the highly sensitive optical stress sensor can be achieved by small $\Delta F / \Delta d$ and $\Delta d / \Delta \lambda$, that is, larger structural variation under a given stress and larger optical spectrum shift under a given structural variation. Actually, we can further exactly define the minimum detectable stress variation (δF, in newton unit) instead of that per wavelength unit by considering the minimum spectral resolution of the measured light wave, which is decided by the measured optical line-width in spectrum, or equivalently, Q factor. Thus we can modify Eq. (1) to be:

$$\delta F = \frac{\Delta F}{\Delta d} \times \frac{\Delta d}{\Delta \lambda} \times \frac{\lambda}{Q} = \frac{\lambda}{SWQ} \tag{2}$$

where λ, Q, and λ / Q represent the wavelength, Q factor, and optical line-width in spectrum, respectively. Therefore, except for small $\Delta F / \Delta d$ and $\Delta d / \Delta \lambda$, high Q factor of the measured light wave is also necessary to achieve small δF. Unfortunately, in present reports, the light wave in PhC membranes, waveguides, and microcavities are with low Q factors (< 1,000) and limit the δF. For simplicity, in the following investigations and discussions, we define factors of $S = \Delta d / \Delta F$ and $W = \Delta \lambda / \Delta d$ to represent the structural variation rate due to the applied stress and wavelength shift rate due to the structural variation, respectively. And the δF can be expressed as λ / SWQ as in Eq. (2).

#104267 - $15.00 USD Received 18 Nov 2008; revised 26 Dec 2008; accepted 8 Jan 2009; published 26 Jan 2009

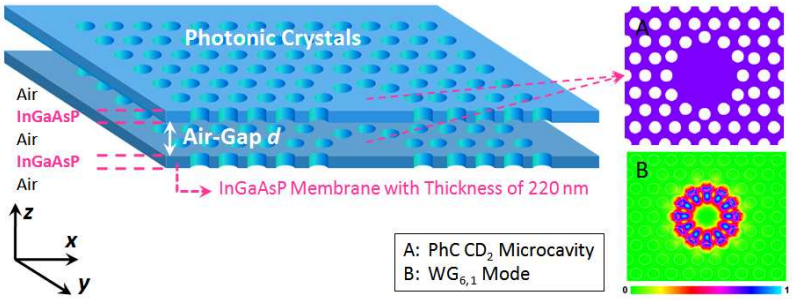

Fig. 1. Scheme of DL PhC microcavity based on PhC CD_2 microcavity design. The PhC CD_2 microcavity and the simulated well-sustained $WG_{6,1}$ mode profile in electrical filed are also shown in the right insets.

3. DL PhC membrane microcavity

In this report, we present a DL PhC membrane microcavity design with air-gap distance d, as shown in Fig. 1, based on the PhC CD_2 microcavity with WG mode in our previous work [16]. The DL PhC microcavity is composed of two identical InGaAsP PhC membranes with thickness and refractive index of 220 nm and 3.4, which sustains single transverse-electrical polarized fundamental mode in each membrane. And the PhC CD_2 microcavity sustaining $WG_{6,1}$ mode (the former and latter sub-numbers denote the azimuthal number and radial order of the WG mode) is designed by shifting the 12 nearest air-holes outward or inward according to the micro-gear effect. The PhC CD_2 microcavity design and $WG_{6,1}$ mode profile in electrical field are both shown in the insets A and B of Fig. 1. First, the modal properties of DL PhC membrane microcavity are investigated by 3D FDTD method. The simulated domain is $24a \times 24a \times 12a$ with $a/16$ computed grid size. And the PhC lattice constant a, air-hole radius r, and d are set to be 420, 135, and 440 nm, respectively. The simulated bonding and anti-bonding modes profiles in electrical field in x-z plane based on $WG_{6,1}$ mode are shown in Figs. 2(a) and (b), which can be analog to the electronic bonding and anti-bonding states in chemical molecules. Actually, this "photonic molecule" design widely considered as the key component to construct optical logic circuits has been investigated in different in-plane micro-structures, for example, micro-sphere [17], micro-cylinder [18], and micro-disk [19]. The vertical coupling of DL structure differed from in-plane coupling in above references is mainly due to the main coupling (loss) direction in PhC microcavity is in the vertical (TIR confinement) direction. This DL structure can be realized by MEMS technologies [20] and is potential in integrating with condensed photonic circuits.

As we mentioned before, to design an optical stress sensor, we need to know the wavelength shift rate $W = \Delta\lambda / \Delta d$ arisen from the structural variation first. In our design, we consider the air-gap distance d between the membranes as the structural variation parameter. In 3D FDTD simulations, d is varied from 165 to 660 nm. The relationship between d and the simulated resonance wavelength λ are shown in Fig. 2(c), which can be directly analog to the relationship between energy states and distance between atoms in chemical molecules. In Fig. 2(c), due to the weakened waveguide evanescence coupling when these two membranes become far apart, the optical mode will tend to act like the original $WG_{6,1}$ mode in single membrane and the wavelength difference between the bonding and anti-bonding modes becomes smaller when d increases. Thus, there will be different wavelength shift rate W under different d and the W factor will decrease when d increases. The calculated W factor at different d is shown in Fig. 3 for the bonding mode. For example, the W factors are found to be 0.235 and 0.007 nm optical spectral shifts of bonding mode for 1 nm air-gap d decreasing when the initial d = 165 and 550 nm, respectively. These values are higher than previous reports [11-13], which also indicate the strong optical spectral response of this DL structure in serving as an optical stress sensor. As a result, we can say that high sensitivity (small δF) can

#104267 - $15.00 USD Received 18 Nov 2008; revised 26 Dec 2008; accepted 8 Jan 2009; published 26 Jan 2009

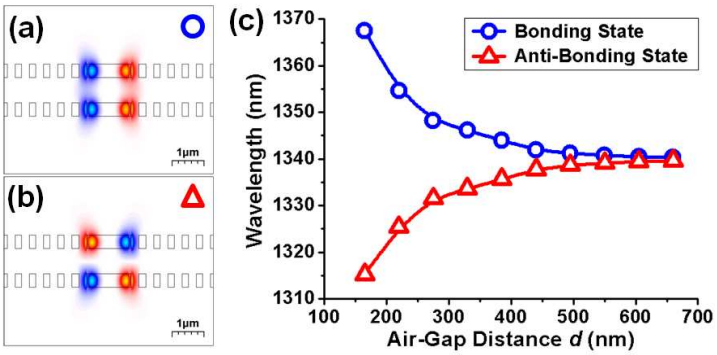

Fig. 2. The simulated mode profiles in electrical field in *x*-*z* plane of (a) bonding and (b) anti-bonding modes. (c) The simulated wavelengths of bonding and anti-bonding modes versus the air-gap distance *d*.

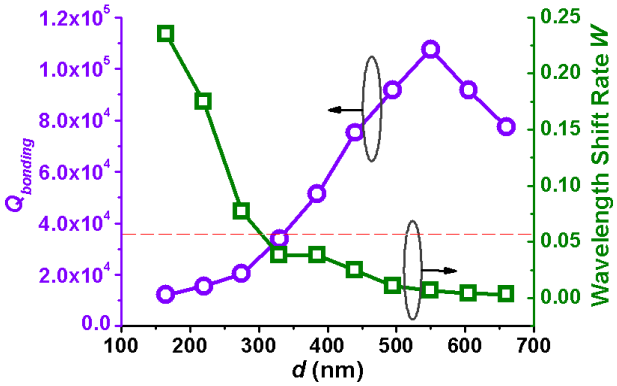

Fig. 3. The simulated $Q_{bonding}$ (open circle) for air-gap distance *d* varied from 165 to 660 nm. High $Q_{bonding}$ ~ 110,000 is obtained when *d* = 550 nm. The wavelength shift rate *W* (open square) under different *d* is also presented, which decreases when the two membranes become far apart. The original *Q* factor (~36,000) of $WG_{6,1}$ mode in single-membrane PhC CD_2 microcavity is also denoted by the red horizontal dash-line.

be achieved in our design by choosing small *d* (large *W* factor). However, as we mentioned in equation (2), in terms of optical properties, the δF is not only determined by the *W* factor but also by the *Q* factor. However, very little attention has been given to the importance of *Q* factor in optical stress sensors in literatures.

Thus, we calculate the *Q* factors of bonding and anti-bonding modes when *d* = 440 nm by the approaches of energy decay and Fourier harmonic analysis with Padé approximation in FDTD simulations. We obtain high *Q* factors of 75,200 and 22,700 from bonding ($Q_{bonding}$) and anti-bonding modes, respectively. The former one is even higher than that of $WG_{6,1}$ mode (~ 36,000) in original PhC CD_2 microcavity. Again, according to equation (2), high *Q* factor is benefit to obtain small δF. Therefore, in the following investigations, we will focus on the bonding mode with high *Q* factor. The simulated $Q_{bonding}$ with *d* varied from 165 to 660 nm is shown in Fig. 3. There are two main effects on $Q_{bonding}$ variation, waveguide evanescence coupling between two PhC membranes and optical coupling to transverse magnetic (TM) mode due to the symmetry breaking for individual PhC membrane. For small *d*, TM mode coupling will contribute extra optical loss and lead to low *Q* factor smaller than that in original PhC CD_2 microcavity. TM mode coupling loss decreases when *d* increases, and we observe a continuous increase of *Q* factor. When *d* is too large, *Q* factor decreases due to weakened waveguide evanescence coupling. As a result, in Fig. 3, we obtain a maximum $Q_{bonding}$ of 110,000 when *d* = 550 nm. Although the highest $Q_{bonding}$ is available when *d* = 550

#104267 - $15.00 USD Received 18 Nov 2008; revised 26 Dec 2008; accepted 8 Jan 2009; published 26 Jan 2009

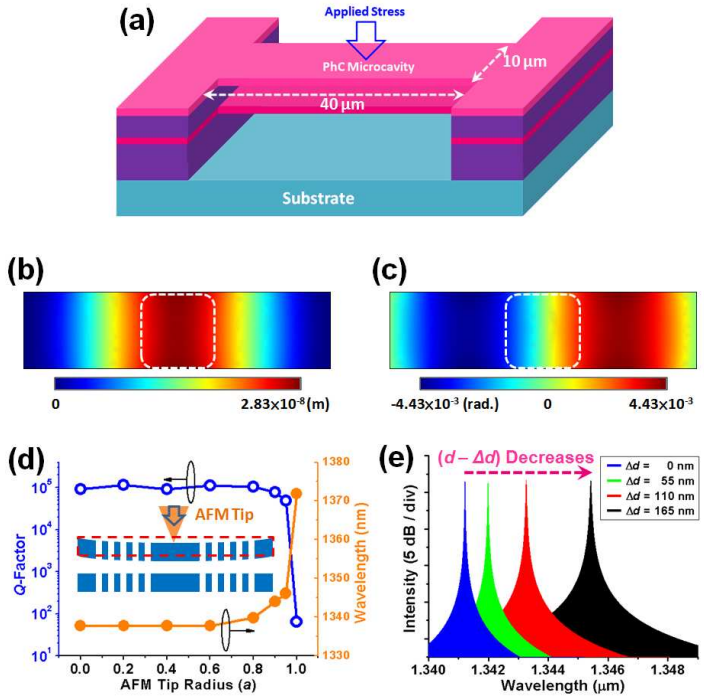

Fig. 4. (a) Scheme of DL PhC microcavity in bridge geometry. The simulated (b) air-gap displacement Δd and (c) torsion distribution of the InGaAsP bridge geometry when F = 50 nN. The torsion mainly distributes at both sides of the bridge from the center. The PhC pattern is denoted by the white dash-line enclosed region. (d) The simulated $Q_{bonding}$ and wavelength variations with d = 495 nm when AFM tip with different diameters contacts the center of the microcavity to apply stress. When the tip size is smaller than 680 nm in diameter, $Q_{bonding}$ will not be affected significantly. (e) The simulated bonding mode wavelength shift when d = 495 nm with Δd increased from 0 to 165 nm.

nm, the W factor at this d value is smaller than the cases with small d. Since the δF in equation (2) depends both on the Q and W factors, we can conclude there will be an optimal design range for small δF according to the trade-off between $Q_{bonding}$ and the W factor.

4. Membrane design and FEM simulated structural variation

So far, we have investigated and obtained the wavelength shift rate W and $Q_{bonding}$ under different d. In this section, we will find the relationship between the applied stress and corresponding structural variation by FEM simulations. First, we present a DL geometric design named bridge, as shown in Fig. 4(a). Both membranes are with thickness, width, and length of 220 nm, 10 μm, and 40 μm, respectively. The PhC CD_2 microcavity patterns are defined at the center of each membrane. This structure can be realized by using a DL epitaxial structure composed of double InGaAsP layers with InP sacrificial layers. After defining the PhC patterns using electron-beam lithography and a series of dry-etching process, the suspended DL membrane structure can be formed by HCl selective wet-etching process. In addition to the DL PhC membrane microcavity, one could insert a pair of side-coupled waveguides for PhC microcavity [16, 21] serving as the input and output channels for optical measurements.

In FEM simulations, the point stress F is applied on the center of top membrane and the induced strain for different geometries will be calculated according to Young's module. The material is assumed to be isotropic, linear, and elastic. The applied stress and supporting are located at the center and two ends of the bridge, respectively, according to the scheme in Fig. 4(a). The structural responses are calculated by solving material elasticity matrix according to

#104267 - $15.00 USD Received 18 Nov 2008; revised 26 Dec 2008; accepted 8 Jan 2009; published 26 Jan 2009

Hoke's Law under Mindlin assumption. Some important parameters of silicon and InGaAsP, including Young's modulus (Y_0), Poisson ratio (σ), density (ρ), and thermal expansion coefficient (T), are listed in Table I. When we design the membrane geometry, two characteristics should be concerned to keep the unnecessary optical influence on PhC microcavity minimum when the stress is applied on the membrane to change the air-gap distance d. First, the air-gap displacement Δd in z-direction in PhC microcavity region should be as uniform as possible to ensure the linear relationship between F and Δd. Second, the torsion in x-y plane should be as small as possible to eliminate the elongation of PhC microcavity and distortion of PhC lattice structure, which may cause unwanted optical losses, such as PBG shift, Q factor degradation, and so on. From FDTD simulation, the in-plane Q factor of $WG_{6,1}$ mode in PhC CD_2 microcavity is close to 10^7 when the number of surrounding PhC periods is larger than 11, that is, to maintain sufficient in-plane PBG confinement, the PhC region should be at least 10×10 μm^2. Thus, the uniform Δd and torsion-free in 10×10 μm^2 PhC region are required. The simulated Δd and torsion distribution when F = 50 nN are shown in Figs. 4(b) and (c). The 10×10 μm^2 PhC region mentioned above is indicated by the white dash-line enclosed region. In Fig. 4(b), reasonably, the maximum displacement Δd_{max} ~ 27.8 nm appears at the center of the bridge, where the stress directly applies. The displacement variation is mainly along the x-direction and the maximum displacement difference (Δd_{max} - Δd_{min}) in the PhC region is 4.5 nm. The uniformity $\Delta d'$ = (Δd_{max} - Δd_{min}) / (Δd_{max} + Δd_{min}) in the PhC region is 8.8 %. On the other hand, from the simulated torsion distribution in Fig. 4(c), significant torsion is observed at both sides of the central region and partial are in the PhC region.

In this bridge geometric design, the stress is directly applied at the center of the microcavity. In experiments, one could demonstrate this by atomic force microscope (AFM) tip probing directly [12] at the center of microcavity, as shown in the inset of Fig. 4(d). To demonstrate this, the applied tip above the microcavity should not induce extra influences on the optical properties of the microcavity. By FDTD simulated Q factor and wavelength variations shown in Fig. 4(d), we can confirm that there will be no significant influence on bonding mode when the tip size is smaller than 680 nm (~ 0.8a) in diameter, which is larger than the size of general AFM tip. This large perturbation tolerance is mainly attributed to the significant zero-field node of WG mode. In addition, we also simulate the bonding mode wavelength shift when d = 495 nm and Δd varied from 0 to 165 nm, as shown in Fig. 4(e). The wavelength and line-width of bonding mode both increase when Δd increases, which agree with the trends of results in Figs. 2(c) and 3.

However, the approach of AFM tip applying stress and the overlap of stress-applying and stress-sensing regions in the bridge geometry will limit the flexibility in realistic situations. Besides, the torsion that may cause influence on lattice structure in the PhC region should be eliminated and the uniformity $\Delta d'$ can be further improved. Thus, we present another geometry named bridge-with-wings (BwWs), as shown in Fig. 5(a). In this BwWs geometric design, the PhC microcavity and the point stress are defined and applied on the wing and bridge regions, respectively. Two wings with PhC patterns are designed in Fig. 5(a) due to the need for structural balance and only one wing is needed in stress sensing. The FEM simulated air-gap displacement Δd and torsion distribution when F = 50 nN are shown in Figs. 5(b) and (c). From the Δd distribution in Fig. 5(b), the maximum displacement difference (Δd_{max} - Δd_{min}) of 3.3 nm in the PhC region is along the y-direction and the uniformity $\Delta d'$ in the PhC region is only 6.6 %, which are slightly improved compared with those in the original bridge geometry. In addition, in Fig. 5(c), the torsion mainly distributes in the bridge region and is close to zero in the wing region, which is much better than that in the bridge geometry. This torsion-free on the wing region is mainly arisen from the width design of neck region as

Table I. Material parameters for silicon and InGaAsP used in FEM simulation.

Material	ρ (kg/m^3)	Y_0 (Pa)	σ	T (1/K)
Silicon	2330	1.31×10^{11}	0.27	4.170×10^{-6}
InGaAsP	4914	6.27×10^{10}	0.35	4.791×10^{-6}

#104267 - $15.00 USD Received 18 Nov 2008; revised 26 Dec 2008; accepted 8 Jan 2009; published 26 Jan 2009

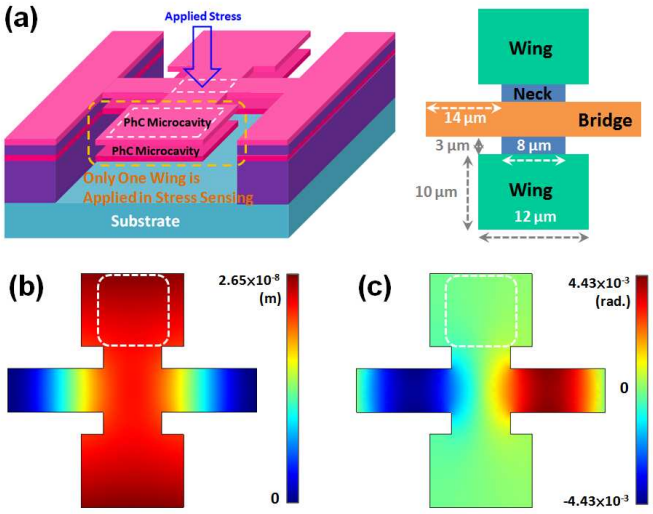

Fig. 5. (a) Scheme of DL PhC microcavity in BwWs geometry. The applied stress and PhC patterns are located in bridge and wing regions, respectively. The simulated (b) air-gap displacement Δd and (c) torsion distribution of the InGaAsP BwWs geometry when F = 50 nN. The PhC pattern is also denoted by the white dash-line enclosed region. The torsion-free regions appear on the wings.

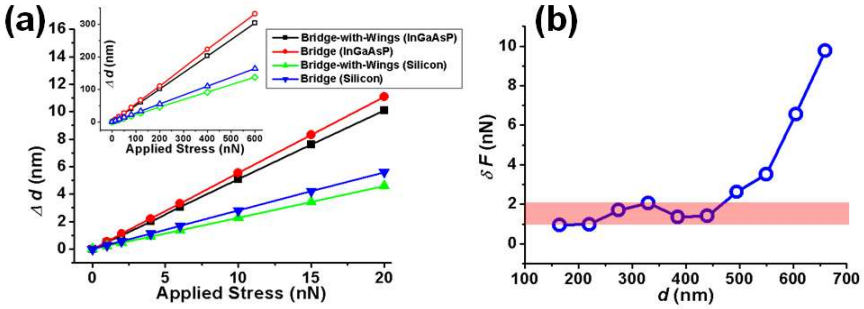

Fig. 6. (a) The simulated relationship between the applied stress and air-gap displacement Δd. The relationships of bridge and BwWs geometries for silicon and InGaAsP materials are presented. (b) The calculated minimum detectable stress variation δF for the BwWs geometry under different air-gap distance d.

shown in Fig. 5(a). When the width of neck region decreases, the torsion will distribute in the bridge region and not extend into the wings. This also indicates the x-y elongation in the PhC region due to torsion can be ignored in this design. Besides, the separation of stress-applying region and stress-sensing region also provides larger tolerance and freedom in operation than the bridge geometry.

From the FEM simulation results of above two DL geometries, we can summarize and obtain the relationship between the applied stress F and the air-gap displacement Δd, as shown in Fig. 6(a). The calculated structural variation rate S of the bridge and BwWs geometries are 0.553 and 0.507 nm / nN, respectively. Due to the smaller volume (weight) of the bridge geometry, larger structural variation than that in the BwWs geometry is obtained under the same F, as shown in Fig. 6(a). We also use silicon material on the same structures for comparison. The simulated results are also shown in Fig. 6(a). The calculated S factors of the

#104267 - $15.00 USD Received 18 Nov 2008; revised 26 Dec 2008; accepted 8 Jan 2009; published 26 Jan 2009

bridge and BwWs geometries are 0.273 and 0.229 nm / nN, respectively, which are twice smaller than those using InGaAsP material. This means that we can have twice structural response for applied stress by using InGaAsP instead silicon under the same geometric design. This is mainly attributed to large Young's modulus of silicon, as listed in Table I. According to equation (2) and combining FEM and FDTD simulations, we can obtain δF from the BwWs geometry when d is varied from 165 to 660 nm, as shown in Fig. 6(b). The smallest δF is only 0.95 nN when d = 165 nm. We also find that the δF can be maintained nearly constant at a low value around 1 to 2 nN under a large range of initial d from 165 to 440 nm as indicated by the shadow region in Fig. 6(b), which provides a large design and fabrication tolerances in keeping high sensitivity for initial d inaccuracy after fabrication. In addition, we also consider the interactions between the two closely-spaced PhC membranes, including van der Waals, Casimir, and radiation forces [22]. For the d values considered here, the van der Waals and Casimir forces inversely proportional to d^7 and d^4 can be neglected compared with δF. On the other hand, the radiation force can be regarded as an offset force in our design under a given d.

Because of the large structural response S and optical response W, the smallest δF value in this DL design is decided by the line-width (Q factor) of the WG mode. Certainly, depending on application requirements, the δF smaller than nN level can be achieved by applying other ultra-high Q micro- and nano-cavity designs [23, 24] to the DL structure. Thus, we believe this DL structure PhC microcavity design is potential and promising in demonstrating ultra-high sensitivity optical stress sensors with large design and fabrication tolerances.

5. Conclusion

In this report, we first present the design principles to obtain a highly sensitive optical stress sensor. Then we present a DL photonic molecule design based on PhC CD_2 microcavity with high Q $WG_{6,1}$ mode. By applying 3D FDTD method, the optical bonding and anti-bonding states in this microcavity structure analog to the energy states in chemical molecule are investigated and addressed. According to the requirements of the design principles, we investigate several properties of this DL PhC microcavity. First, by varying the air-gap distance d, we simulate the corresponding wavelength variation of bonding mode. The optical wavelength shift rates W are 0.235 and 0.007 nm spectral shifts for 1 nm air-gap d decreasing when d = 165 and 550 nm, respectively, which are much higher than those in recent reports. Second, the $Q_{bonding}$ variations under different d are investigated. We obtain high $Q_{bonding}$ of 110,000 in DL PhC microcavity design when d = 550 nm. This high Q factor increases the spectral resolution and sensitivity in serving as an optical stress sensor. Third, by applying FEM, we propose two DL geometric designs, bridge and BwWs, and investigate their structural responses S due to the applied stress. We obtain high S value of 0.507 nm / nN from InGaAsP BwWs geometry, which is twice sensitive than the same DL geometry using silicon material. From above results for our proposed DL PhC microcavity, we obtain large optical response due to the DL structural variation, high Q factor that leads to fine resolution in optical spectrum, and large structural response due to the applied stress, which are all beneficial for realizing highly sensitive optical stress sensors. The minimum detectable stress variation δF is estimated to be as small as 0.95 nN when d = 165 nm. Besides, the δF can be maintained nearly constant at a low value around 1 to 2 nN under a large range of initial d from 165 to 440 nm, which provides large design and fabrication tolerances. This DL PhC membrane microcavity structure is very promising and feasible for optical stress sensor applications. Further improved sensitivity can be obtained by employing PhC micro- and nano-cavities with ultra-high Q factors if required.

Acknowledgments

This work is supported by Taiwan's National Science Council (NSC) under contract numbers NSC-97-2120-M-009-004 and NSC-95-2221-E-009-056-MY3. The authors would like to thank the help from Center for Nano Science and Technology (CNST) of National Chiao Tung University, Taiwan.

#104267 - $15.00 USD Received 18 Nov 2008; revised 26 Dec 2008; accepted 8 Jan 2009; published 26 Jan 2009